Journal Pre-proof

Nuclear and magnetic structures of $KMnF_3$ perovskite in the temperature interval 10□K–105□K

Kevin S. Knight, Dmitry D. Khalyavin, Pascal Manuel, Craig L. Bull, Paul McIntyre

PII: S0925-8388(20)32299-4

DOI: https://doi.org/10.1016/j.jallcom.2020.155935

Reference: JALCOM 155935

To appear in: *Journal of Alloys and Compounds*

Received Date: 6 May 2020

Revised Date: 3 June 2020

Accepted Date: 4 June 2020

Please cite this article as: K.S. Knight, D.D. Khalyavin, P. Manuel, C.L. Bull, P. McIntyre, Nuclear and magnetic structures of $KMnF_3$ perovskite in the temperature interval 10□K–105□K, *Journal of Alloys and Compounds* (2020), doi: https://doi.org/10.1016/j.jallcom.2020.155935.

Kevin S. Knight: Conceptualization, Investigation, Writing - original draft, Writing - review and editing.

Dmitry D. Khalyavin: Conceptualization, Investigation, Writing - original draft.

Pascal Manuel: Investigation.

Craig L. Bull: Investigation.

Paul McIntyre: Resources.

Nuclear and magnetic structures of $KMnF_3$ perovskite in the temperature interval 10 K – 105 K

Kevin S. Knight,[a,b,*] Dmitry D. Khalyavin,[c] Pascal Manuel,[c] Craig L. Bull,[c] and Paul McIntyre[c]

[a] *Department of Earth Sciences, University College London, Gower Street, London, WC1E 6BT, United Kingdom*

[b] *Department of Earth Sciences, The Natural History Museum, Cromwell Road, London, SW7 5BD, United Kingdom*

[c] *ISIS Neutron Spallation Source, Rutherford Appleton Laboratory, Harwell Campus, Didcot, Oxfordshire, OX11 0QX, United Kingdom*

* Corresponding author

E-mail address: kevinstevenknight@gmail.com

ABSTRACT

The nuclear and magnetic structures of the perovskite-structured compound $KMnF_3$ have been investigated using high resolution neutron powder diffraction techniques for the first time. Data have been collected in 1 K intervals from 105 K to 10 K to characterize previously identified structural phase transitions from Phase II (space group *I*4/*mcm*) – (88 K) Phase III (space group *Cmcm*) – (82 K) Phase IV (space group *Pnma*) using the diffractometer HRPD. In the temperature interval 91 K ≥ T ≥ 75 K, $KMnF_3$ exhibits a temperature-dependent phase coexistence between phases with space groups *I*4/*mcm* and *Pnma*, contrary to the earlier interpretation, with no evidence found for a discrete phase with space group *Cmcm*. A recent revision of the space group of phase IV from *Pnma* to $B2_1/m$ is critiqued and shown to be inconsistent with the neutron diffraction data. The magnetically ordered phases of $KMnF_3$, collinear antiferromagnet for 81.5 K ≤ T ≤ 88.3 K, and canted antiferromagnet with a ferromagnetic component for T ≤ 81.5 K, have been investigated in detail in the temperature interval 90 K – 83 K, in 0.2 K steps using the cold neutron diffractometer WISH, supplemented by lower temperature measurements using HRPD. At a temperature of ~86.8 K, magnetic scattering is observed consistent with the development of a *G*-type spin configuration in the majority tetragonal phase with a moment direction parallel to the *c*-axis, propagation vector **k** = **0**, magnetic space group *I*4/*mcm*. Below 75 K, in the pure orthorhombic phase, $KMnF_3$ is found to inherit the *G*-type ordering parallel to ***c*** in magnetic space group *Pn′ma′* which in addition permits *A*-type antiferromagnetic ordering, and ferromagnetic ordering along the *a*- and *b*-axes respectively.

Keywords: Magnetically ordered materials, Crystal structure, Phase transitions, Neutron diffraction

1. Introduction

By contrast to the voluminous literature concerning the structural and magnetic phase transitions in oxygen-based perovskite-structured compounds, few halogen-based perovskites have been the subject of such detailed investigations [1]. The exceptions to this generalisation have been the studies carried out on the antiferromagnetically ordered phases of $KCuF_3$ and $KMnF_3$ [1]. In the former, there is consensus regarding the low temperature crystallography and its influence on the magnetic behaviour. However, in the latter, despite over 500 publications concerning the physical properties of the compound, its magnetic and structural phase transitions, there remains no detailed crystallographic study of $KMnF_3$ at temperatures below the Néel temperature upon which to base experimental interpretations. Static susceptibility measurements of powdered $KMnF_3$ have shown it to become antiferromagnetically ordered at a temperature of ~88 K [2-4]. Later, more detailed investigations found an additional magnetic transition with a weak ferromagnetic component below ~81 K, transforming to the previously identified collinear antiferromagnetic phase [5]. The space group of the lowest temperature phase of $KMnF_3$ was identified as *Pbnm* (non-standard setting of space group *Pnma*) from single crystal X-ray diffraction data collected at 15 K [6], with *G*-type antiferromagnetic ordering identified from low resolution neutron powder diffraction data collected at 4.2 K [7]. In addition to the magnetic phase transitions, low temperature structural phase transitions were identified from single crystal X-ray diffraction data at ~184 K and ~84 K [6, 8]; both phases were believed to have space group *Pbnm* although single crystal data collected below the Néel temperature suggested a monoclinic pseudocubic sub-cell inconsistent with *Pbnm* [9]. The presence of these structural phase transitions was subsequently confirmed by heat capacity measurements [10-14] which indicated both were first order in character. Neutron inelastic scattering experiments found the 184 K phase transition to be the result of the softening of a single component of the triply degenerate phonon mode with irreducible representation R_4^+ to a crystal structure in space group *I*4/*mcm* [15, 16] contradicting the earlier crystallographic analysis [8]. Further inelastic neutron scattering measurements showed the lower temperature phase transition to be associated by the softening of the singlet phonon mode with irreducible representation M_3^+ [17], and importantly, that the phase transition was first order, and that the phase transition temperature (T_c) and the Néel (T_N) temperature did not coincide with $T_c > T_N$. The crystallographic aspects of the two highest temperature phases have long been in agreement [5, 8, 18], the space group assignments of the lowest temperature phases has been inferred from the presence of superlattice reflections at the R, and M points of the pseudocubic Brillouin zone, rocking curves of the 004 reflection as a function of temperature, and by appealing to group theoretical arguments [17, 19, 20]. In the most recent investigation of the magnetic, elastic, and anelastic behaviour of $KMnF_3$ below room temperature, three phase transitions were identified [19]: Phase I (space group $Pm\bar{3}m$ (190 K) – Phase II (space group *I*4/*mcm*) – (88 K) Phase III (space group *Cmcm*, collinear antiferromagnet) – (82 K) Phase IV (space group *Pnma*, canted antiferromagnet).

The existence of a discrete phase III in the temperature interval 82 K - 88 K has only been inferred by non-structural specific techniques, magnetization [19] and static susceptibility [2-4], and a rocking curve around a single reciprocal lattice vector [20] which is insufficient to characterize a ferroelastic distortion to a new crystallographic phase. As stated earlier, the space group of this phase was deduced from the application of group theoretical techniques to deduce the likely ascent in symmetry from phase IV, believed to be in space group *Pnma* [19].

The space group assignment of the lowest temperature phase, however, remains controversial and has recently been revised as monoclinic $B2_1/m$ (non-standard setting of space group $P2_1/m$) from analysis of the line shape of a limited number of low index reflections using laboratory source X-ray powder diffraction data [21]. A crystal structure in this revised space group was derived by profile refinement of laboratory source X-ray powder diffraction data collected at 12 K [21]. The symmetry lowering associated with the monoclinic space group from the orthorhombic space group *Pnma* results in two independent potassium and manganese sites, and four independent fluorine sites [21]. However, detailed re-assessment of the crystal structure of $KMnF_3$ derived from the 12 K X-ray diffraction data show it to be crystal-chemically implausible with the two chemically equivalent Mn^{2+} octahedra exhibiting sheared morphologies and significantly different polyhedral volumes, bond valence sums, quadratic elongations, and octahedral angle variance. Mn - F bond lengths range from too short, 1.893(1) Å, to too long, 2.379(1) Å. Furthermore, in reassigning the space group to $P2_1/m$, only the line shape of two reflections were assessed, and observed violations of the systematic absence conditions of space group *Pnma* from the two glide planes, which would be proof of the symmetry descent, were not considered.

In the nuclear and magnetic structural study of $KMnF_3$ reported here, we reinvestigate the nature of phases III and IV using high resolution neutron powder diffraction techniques for the first time. Nuclear and magnetic structures for the collinear antiferromagnetic phase and the canted antiferromagnetic phase are reported. The current investigation corrects many of the conclusions of the earlier, non-structural specific techniques.

2. Experimental

Phase pure $KMnF_3$ was synthesised using standard solution techniques [22] from reactant aqueous solutions of KF and $MnCl_2$ according to the reaction shown below.

$$3KF(aq) + MnCl_2(aq) \rightarrow KMnF_3(s) + 2KCl(aq).$$

The filtered $KMnF_3$ precipitate was washed using de-ionised water and filtered a further three more times to remove any remaining soluble KCl, before being finally dried at 100° C in a muffle furnace. The dried powder was then annealed at 700° C under an argon atmosphere

for 24 hours, before being lightly ground to produce a sample suitable for powder diffraction investigations.

We have reassessed the nuclear and magnetic structures of $KMnF_3$ between 10 K and 300 K using high resolution neutron powder diffraction utilising two time-of-flight diffractometers, HRPD [23] and WISH [24] at the ISIS source of the Rutherford Appleton Laboratory. The advantage of neutron powder diffraction over X-ray powder diffraction for structural characterization lies particularly in the light atom sensitivity of the former over the latter, and this is particularly important in perovskite crystallography where the presence/absence of the superlattice reflections at the R, M and X points of the pseudocubic Brillouin zone are diagnostic and arise principally from anion displacements. In addition, the approximately Q-independent resolution function of long flightpath time-of-flight diffractometers in backscattering permits simple assessment of the line splitting associated with the fundamental Bragg reflections at structural phase transitions.

Time-of-flight data were collected using the full 40 ms time frame of WISH running at 10Hz, and in two 100 ms windows (30 - 130 ms, 100 - 200 ms) for HRPD also running at 10 Hz. Data were normalised and corrected for self-shielding using in-house software to produce reduced datasets suitable for profile refinement.

3. Results and discussion

3.1 Crystal structure of the lowest temperature phase

In Figure 1, two diagnostic regions of the HRPD data are illustrated, showing the observed data collected at 10 K (upper) compared to the calculated pattern (lower) based on the refined and revised crystal structure in space group $P2_1/m$ ($B2_1/m$) [21]. Figure 1a shows that the strongest calculated systematic absence violation reflections of space group *Pnma* 021 (n-glide) and 120 (a-glide) at ~ 3.4 Å are not present in the measured data, and also that the strong calculated fundamental reflections 111, and $1\bar{1}1$ at ~ 3.73 Å from the monoclinic model are also unobserved. Figure 1b shows the observed and calculated intensity around the pseudocubic 200 reflection, with the approximate widths of the resolution functions of the two instruments shown as horizontal lines. It is clear from this Figure that the calculated triplet is inconsistent with the observed neutron diffraction data, and taking this, and the results illustrated in Figure 1a into account, the revision of the low temperature space group of $KMnF_3$ from *Pnma* to $P\ 1\ 2_1/m\ 1$ is clearly incorrect. The crystal structure at 10 K, derived from profile refinement of the neutron diffraction data, shows the single MnF_6 octahedron to be essentially regular with bond lengths of 2.0992(3) Å, 2.099(1) Å, and 2.097(1) Å and not the irregular, sheared octahedra derived from the X-ray diffraction data. Crystallographic results for $KMnF_3$ at 10 K are listed in Table 1 along with results from the tetragonal phase at 140 K, and the cubic phase at 235 K.

The revision of the space group of $KMnF_3$ is identical to the correction of the space group of $KCaF_3$ at 300 K from $B2_1/m$ (laboratory X-ray diffractometer) back to the originally designated space group *Pnma* (HRPD neutron time-of-flight diffractometer) [25].

3.2 Magnetic structure determination of the collinear antiferromagnetic phase

To fully characterize the phase transitions from the intermediate temperature (190 K > T > 88 K) tetragonal phase into the *Pnma* phase, data were collected using HRPD in the range 105 K ≥ T ≥ 10 K in 1 K steps. On the basis of the analysis of the temperature dependence of the 400 X-ray rocking curve [20], a first order phase transition from the *I*4/*mcm* tetragonal phase to an orthorhombic phase in space group *Cmcm* was expected with the concomitant development of superlattice reflections at the M and X points of the pseudocubic Brillouin zone, and the intensity of the pseudocubic 200 reflection to change from a doublet to a triplet of approximately equal intensities [26]. Figure 2 illustrates the pseudocubic 200 reflection at three temperatures, 105 K in the *I*4/*mcm* phase, 80 K in the nominal *Cmcm* phase, and 65 K in the *Pnma* phase. It is evident from this Figure that at 80 K, instead of the triplet with essentially identical full widths at half maximum intensity indicative of a discrete phase in space group *Cmcm*, we have coexistence of the high and low temperature phases of $KMnF_3$ in space groups *I*4/*mcm* and *Pnma*. Furthermore, as the unit cell volumes of the *I*4/*mcm* and *Pnma* phases are to a good approximation equal, the volume phase fractions of both phases can be determined from integrating the relevant intensity contributions of each to the pseudocubic 200 reflection, the results are shown in Figure 3a. The integrated intensities of the pseudocubic 200 reflection are essentially identical for both phases in their respective single phase regions, and, as the sum of the individual intensity contributions is the same for the coexistence region, we have confidence in our determination of the volume fraction, which is illustrated in Figure 3b. As a guide to the eye, these data have been fitted empirically to a three parameter sigmoidal function: volume fraction *I*4/*mcm* phase = $a/(1 + \exp(-(T - T_0)/b))$ where a = 0.942(7), T_0 = 80.09(6) K, and b = 1.89(5) K. Furthermore, as the unit cell volumes for the two phases within the coexistence region are to first order identical, the volume fraction of a phase is to a good approximation equivalent to its weight fraction.

Note, for reasons outlined below, HRPD is not the ideal instrument for magnetic structure fitting or refinement, and hence we have not carried out a full magnetic and structural multiphase profile refinement to determine the phase fractions of the two phases as we would have carried out for non-magnetic materials (for example see the results of multiphase fitting to the low temperature data collected on HRPD from $RbCaF_3$ in the *I*4/*mcm* and *Pnma* phase coexistence region [27]).

The origin of the collinear antiferromagnetism was determined from the normalization of the purely magnetic 101 reflection (indexed on the tetragonal unit cell) to the weight fraction of the *Pnma* phase as illustrated in Figure 4. The magnetic intensity reduces with increasing temperature as shown by the fit to a critical exponent for the data below 72 K which is shown as the full line on the figure. Above this temperature, in the phase coexistence region, the magnetic intensity increases rapidly before abruptly falling to zero at the Néel

temperature. We therefore conclude that the majority tetragonal phase becomes antiferromagnetically ordered in the coexistence field, and a preliminary magnetic profile refinement using the HRPD data suggested a collinear arrangement of Mn moments oriented parallel to ***c***.

HRPD is, however, specifically designed for crystallographic analysis, and the instrument lacks a large solid angle detector at low scattering angle and the high flux at long neutron wavelengths that are necessary for precise magnetic structure determination and refinement in time-of-flight instrumentation. To confirm the onset of a long-range magnetic ordering in the tetragonal phase around 88K, detailed neutron diffraction data were collected in the temperature range of 90 K > T > 83 K with 0.2 K steps using the high-resolution cold neutron diffractometer WISH [24]. The measurements were carried out on cooling to stabilize as much the tetragonal phase as possible below the critical temperature. The integrated intensity of the 101 reflection (indexed on the tetragonal unit cell) as a function of temperature is shown in the inset of Figure 5b. This reflection is forbidden in the *I4/mcm1'* space group, and only magnetic scattering is expected there for the case of a *G*-type spin configuration. Below T_{N1} ~ 86.8K, a detectable intensity for this reflection was observed, demonstrating a critical behaviour typical of continuous magnetic phase transitions. A quantitative refinement of the patterns, as illustrated in Figure 5, revealed that the data can only be satisfactorily fitted assuming *G*-type antiferromagnetic ordering for the major tetragonal phase (phase fraction ~ 86(1)% at 85 K) with Mn moments parallel to ***c***. Attempts to refine the data in a model where only the minor orthorhombic phase is magnetically ordered gave poor quality fits with a resultant unreasonably large magnetic moment. The onset of the magnetic state in the minority orthorhombic phase in the 83 K < T < 90 K temperature range could not be reliably determined from these diffraction data because the phase fraction is so low. The quality of the data, however, was sufficient to unambiguously determine the spin direction in the tetragonal phase to be along the *c*-axis (Figure 5 a, b). With reference to the tetragonal cell, the magnetic ordering has $\boldsymbol{k} = \mathbf{0}$ propagation vector and the G_z-antiferromagnetic configuration, thus yielding the *I4/mcm* magnetic space group (Figure 6 a). The magnetic symmetry does not allow any spin canting in agreement with the magnetization data reported by Carpenter *et al*. [19] for the relevant temperature range.

3.3 Magnetic structure determination of the Pnma phase

The *G*-type spin configuration is inherited by the low temperature orthorhombic phase stable below 75 K. The ordered moment ~4.8(2) μ_B at T = 10 K has been found to be along the *c*-axis (G_z-mode), resulting in the *Pn'ma'* magnetic space group (Figure 6 b). This symmetry allows a spin canting with *A*-type antiferromagnetic and ferromagnetic components along the *a*- and *b*-axes, respectively. Although the values of these orthogonal spin components are beyond the detection limit of the diffraction experiment, the presence of the latter is fully consistent with the reported magnetization measurements [19]. A precise determination of the critical temperature T_{N2} for the magnetic phase transition of the orthorhombic phase is impossible from the available diffraction data from WISH, but apparently, it is very close to the onset of the transition to the tetragonal phase. The power

law fit to the magnetic intensity derived from the HRPD data illustrated in Figure 4 suggests T_{N2} to be ~77(1) K.

3.4 Comparison of the magnetic structures

The *G*-type antiferromagnetic ordering found in both tetragonal and orthorhombic phases of $KMnF_3$ is naturally expected for the isotropic 180-degree superexchange interactions between the high-spin Mn^{2+} cations [28]. The corresponding electronic configuration, $e_g^2 t_{2g}^3$ ($S = 5/2$, $L = 0$), also implies that, to a good approximation, the orbital moment is quenched and the mechanism dominating the magnetic anisotropy is not obvious. It has been shown that in many Fe^{3+}-based complex perovskites, where the iron ions adopt the identical electronic configuration to Mn^{2+}, antisymmetric exchange, $\boldsymbol{D_{ij}}\cdot[\boldsymbol{S_i}\times\boldsymbol{S_j}]$, is the dominant anisotropic interaction, controlling the spin direction in the structure [29, 30]. The primary structural distortions, which activate the antisymmetric exchange between neighbouring spins, $\boldsymbol{S_i}$ and $\boldsymbol{S_j}$, and couple orthogonal spin modes, are octahedral tilting [30-32]. The relevant part of the Dzyaloshinskii vector $\boldsymbol{D_{ij}}$ is along the tilting axis and is proportional to the antiferroaxial vector $\boldsymbol{D_{ij}} \sim \boldsymbol{A_i}\text{-}\boldsymbol{A_j}$, where $\boldsymbol{A_i}$ and $\boldsymbol{A_j}$ are the axial vectors representing rotation of the octahedra on the i_{th} and j_{th} sites. In the tetragonal *I*4*/mcm* phase of $KMnF_3$, the MnF_6 octahedra are tilted about the *c*-axis, implying that the antisymmetric term vanishes, since the spins in the primary G_z-mode are aligned along this direction ($\boldsymbol{S_i}$ and $\boldsymbol{S_j} \parallel \boldsymbol{D_{ij}^{out}}$). This result directly points to the dominant role of the single ion anisotropy.

The situation, however, is different for the orthorhombic *Pn'ma'* phase, where the out-of-phase and in-phase octahedral tilting takes place about the *a*- and *b*-axes, respectively. In this case, the *c*-axis is the spin direction, which optimises the antisymmetric terms imposed by these largest structural distortions ($\boldsymbol{S_i}$ and $\boldsymbol{S_j} \perp \boldsymbol{D_{ij}^{out}}$ and $\boldsymbol{D_{ij}^{in}}$), through the coupling to the orthogonal F_z and A_x magnetic modes [30]. These symmetry arguments combined with the experimentally found spin configuration in the orthorhombic structure of $KMnF_3$, strongly suggest that the antisymmetric exchange dominates the magnetic anisotropy in this phase.

Thus, the experimentally found magnetic structures in the tetragonal and orthorhombic phases of $KMnF_3$ (Figure 6) reveals a competition between the single ion anisotropy and antisymmetric exchange. This competition implies a possibility of unusual spin-flop transition in the tetragonal phase by applying an in-plane magnetic field. In spite of the fact that the field is perpendicular to the spins in the antiferromagnetic G_z-mode, flipping the spin direction to the in-plane configuration, (keeping them perpendicular to the field) will allow the system to generate an additional ferromagnetic component parallel to the field, through the antisymmetric exchange.

4. Conclusions

High resolution neutron powder diffraction in the temperature interval 10 K - 105 K has shown $KMnF_3$ to undergo two magnetic phase transitions at T_{N1} ~ 86.8K, and T_{N2} ~77(1) K, and a single first order structural phase transition from space group *Pnma* to *I*4/*mcm*. A

collinear antiferromagnetically ordered intermediate phase with space group *Cmcm* that was believed to exist between the *Pnma* and *I*4/*mcm* phases has been shown not to exist. Instead, the strongly first order phase transition results in a significant region of phase coexistence between the *Pnma* and *I*4/*mcm* phases (~90 K < T < ~75 K), and within this region ($T < T_{N1}$) the majority tetragonal phase antiferromagnetically orders with a collinear G_z magnetic structure in Shubnikov group *I*4/*mcm*. Below T_{N2} $KMnF_3$ develops a canted antiferromagnetic structure in Shubnikov group *Pn'ma'*. To our knowledge, the presence of a continuous magnetic transition in a material undergoing a first order structural phase transition is unique and would merit further investigation.

Acknowledgements

We are grateful to the two anonymous reviewers for their comments and improvements to the manuscript. Prof. Ludwig Schulz is thanked for editorial handling of the manuscript. Neutron beam time was provided by the Science and Technology Facilities Council.

References

[1] L. Clark, P. Lightfoot, magnetic properties of transition metal fluoride perovskites, in: Photonic and Electronic Properties of Fluoride Materials: Progress in Fluorine Science Series, Elsevier, Amsterdam, 2016.

[2] R.L. Martin, R.S. Nyholm, N.C. Stephenson, Antiferromagnetism in complex fluorides with perovskite structures, Chemistry and Industry 3 (1956) 83 - 85.

[3] S. Ogawa, Antiferromagnetism in $KMnF_3$, J. Phys. Soc. Jpn. 14 (1959) 1115.

[4] K. Hirakawa, K. Hirakawa, T. Hashimoto, Magnetic properties of potassium iron group fluorides KMF_3, J. Phys. Soc. Jpn. 15 (1960) 2063 - 2068.

[5] A.J. Heeger, O. Beckman, A.M. Portis, Magnetic properties of $KMnF_3$. II. Weak ferromagnetism, Phys. Rev. 123 (1961) 1652 - 1660.

[6] O. Beckman, K. Knox, Magnetic properties of $KMnF_3$. I. Crystallographic studies, Phys. Rev. 121 (1961) 376 - 380.

[7] V. Scatturin, L. Corliss, N. Elliott, J. Hastings, magnetic structures of 3d transition metal double fluorides, K*Me*F_3, Acta Crystallogr. 14 (1961) 19 - 26.

[8] O. Beckman, I. Olovsson, K. Knox, Structural changes of $KMnF_3$ at low temperature, Acta Crystallogr. 13 (1960) 506.

[9] A. Okazaki, Y. Suemune, T. Fuchikami, The crystal structures of $KMnF_3$, $KFeF_3$, $KCoF_3$, $KNiF_3$ and $KCuF_3$, J. Phys. Soc. Jpn. 14 (1959) 1823 - 1824.

[10] R.V.G. Rao, C.D. Das, H.V. Keer, A.B. Biswas, The heat capacities of potassium manganese trifluoride, Proc. Phys. Soc. London 81 (1963) 191 - 192.

[11] C. Deendas, H.V. Keer, R.V.G. Rao, A.B. Biswas, Heat capacity of potassium manganese trifluoride, Br. J. Appl. Phys. 17 (1966) 1401 - 1404.

[12] V.G. Khlyustov, I.N. Flerov, A.T. Silin, A.N. Sal'nikov, Heat capacity of $KMnF_3$, Fiz. Tverd. Tela 14 (1972) 175 - 177.

[13] N. Akutsu, H. Ikeda, Specific heat capacities of CoF_2, MnF_2 and $KMnF_3$ near the Néel temperatures, J. Phys. Soc. Jpn. 50 (1981) 2865 - 2871.

[14] W.D. McCormick, K.I. Trappe, Heat capacity measurements of $KMnF_3$ at the soft mode and magnetic phase transitions, in: K.D. Timmerhaus, W.J. O'Sullivan, E.F. Hammel (Eds.) Low temperature Physics LT13, Springer, Boston, 1974, pp. 360 - 364.

[15] V.J. Minkiewicz, G. Shirane, Soft modes in $KMnF_3$, J. Phys. Soc. Jpn. 26 (1969) 674 - 680.

[16] V.J. Minkiewicz, Y. Fujii, Y. Yamada, X-ray scattering and the phase transition of $KMnF_3$ at 184 K, J. Phys. Soc. Jpn. 28 (1970) 443 - 450.

[17] G. Shirane, V.J. Minkiewicz, A. Linz, Neutron scattering study of the lattice dynamical phase transitions in $KMnF_3$, Solid State Commun. 8 (1970) 1941 - 1944.

[18] A. Okazaki, Y. Suemune, The crystal structures of $KMnF_3$, $KFeF_3$, $KCoF_3$, $KNiF_3$ and $KCuF_3$ above and below their Néel temperatures, J. Phys. Soc. Jpn. 16 (1961) 671 - 675.

[19] M.A. Carpenter, E.K.H. Salje, C.J. Howard, Magnetoelastic coupling and multiferroic ferroelastic/magnetic phase transitions in the perovskite $KMnF_3$, Phys. Rev. B 85 (2012) 224430.

[20] A. Gibaud, S.M. Shapiro, J. Nouet, H. You, Phase diagram of $KMn_{1-x}Ca_xF_3$ ($x < 0.05$) determined by high-resolution x-ray scattering. Phys. Rev. B 44 (1991) 2437 - 2443.

[21] J. Kapusta, P. Daniel, A. Ratuszna, revised structural phase transitions in the archetype $KMnF_3$ perovskite crystal, Phys. Rev. B 59 (1999) 14235 - 14245.

[22] R.H. Langley, C.K. Schmitz, M.B. Langley, The synthesis and characterization of some fluoride perovskites, J. Chem. Educ. 61 (1984) 643 - 645.

[23] A.D. Fortes, A.S. Gibbs, HRPD-X, a proposed upgrade to the ISIS high-resolution powder diffractometer, J. Neutron Res. in press, doi: 10.3233/JNR-190130.

[24] L.C. Chapon, P. Manuel, P.G. Radaelli, C. Benson, L. Perrott, S. Ansell, N.J. Rhodes, D. Raspino, D. Duxbury, E. Spill, J. Norris, Wish: The New Powder and Single Crystal

Magnetic Diffractometer on the Second Target Station, Neutron News 22 (2011) 22 - 25.

[25] K.S. Knight, C.N.W. Darlington, I.G. Wood, The crystal structure of $KCaF_3$ at 4.2 and 300 K: A re-evaluation using high-resolution powder neutron diffraction, Powder Diffraction 20 (2005) 7 - 13.

[26] C.J. Howard, H.T. Stokes, Group theoretical analysis of octahedral tilting in perovskites, Acta Crystallogr. B54 (1998) 782 - 789.

[27] K.S. Knight, A high-resolution neutron powder diffraction study of the low-temperature structural phase transitions in $RbCaF_3$ perovskite, Journal of Solid State Chemistry 263 (2018) 172 - 181.

[28] J.B. Goodenough, Magnetism and the Chemical Bond, Interscience, New York, 1963.

[29] D.D. Khalyavin, A.N. Salak, A.B. Lopes, N.M. Olekhnovich, A.V. Pushkarev, Yu.V. Radyush, E.L. Fertman, V.A. Desnenko, A.V. Fedorchenko, P. Manuel, A. Feher, J.M. Vieira, M.G.S. Ferreira, Magnetic structure of an incommensurate phase of La-doped $BiFe_{0.5}Sc_{0.5}O_3$: Role of antisymmetric exchange interactions, Phys. Rev. B 92 (2015) 224428.

[30] D.D. Khalyavin, A.N. Salak, P. Manuel, N.M. Olekhnovich, A.V. Pushkarev, Yu.V. Radysh, A.V. Fedorchenko, E.L. Fertman, V.A. Desnenko, M.G.S. Ferreira, Antisymmetric exchange in La-substituted $BiFe_{0.5}Sc_{0.5}O_3$ system: symmetry adapted distortion modes approach, Z. Kristallogr. Cryst. Mater. 230(2015) 767 - 774.

[31] L. Bellaiche, Z. Gui, I.A. Kornev, A simple law governing coupled magnetic orders in perovskites, J. Phys.: Condens. Matter 24 (2012) 312201.

[32] D.D. Khalyavin, A.N. Salak, N.M. Olekhnovich, A.V. Pushkarev, Yu.V. Radyush, P. Manuel, I.P. Raevski, M.L. Zheludkevich, M.G.S. Ferreira, Polar and antipolar polymorphs of metastable perovskite $BiFe_{0.5}Sc_{0.5}O_3$, Phys. Rev. B 89 (2014) 174414.

Table 1.
Crystallographic data for the three phases of $KMnF_3$.

Structural parameters	*Pbnm*	*I*4/*mcm*	$Pm\bar{3}m$
	10 K	140 K	235 K
Lattice Parameters/Å			
a	5.90193(6)	5.89907(2)	4.18538(1)
b	5.88848(6)	*a*	*a*
c	8.34826(9)	8.38022(5)	*a*
Unit cell volume/Å^3	290.137(7)	291.624(2)	73.3170(3)
K			
x	0.0052(8)		
y	0.5124(4)		
100u_{iso}/Å^2	0.929(25)	1.52(3)	2.04(3)
Mn			
100uiso/Å^2	0.899(21)	1.04(3)	1.11(3)
moment/μ_B	4.8(2)		
F1			
x	-0.0381(4)		
y	-0.0026(4)		
100u_{11}/Å^2	0.66(8)	2.86(6)	
100u_{22}/Å^2	1.50(8)	u_{11}	
100u_{33}/Å^2	0.83(8)	0.96(7)	
100u_{12}/Å^2	0.26(8)		
100u_{eq}/Å^2	1.00	2.22	
F2			
x	0.2278(2)	0.2257(1)	
y	0.2726(1)	0.2743(1)	
z	0.0180(2)		
100u_{11}/Å^2	1.13(5)	1.47(3)	0.91(4)
100u_{22}/Å^2	1.03(4)	u_{11}	3.77(3)
100u_{33}/Å^2	1.91(7)	2.93(5)	u_{22}
100u_{12}/Å^2	-0.33(4)	-0.70(4)	
100u_{13}/Å^2	-0.06(5)		
100u_{23}/Å^2	-0.05(5)		
100u_{eq}/Å^2	1.36	1.95	2.82
K - F1/Å	2.867(3), 2.758(6)	2.94954(1)	2.95951(1)
K - F2/Å	2.733(3), 2.929(3) 2.916(3)	2.8168(5)	
Mn - F1/Å	2.0992(3)	2.09506(1)	2.09269(1)
Mn - F2/Å	2.099(1), 2.097(1)	2.09547(8)	

Pbnm K, F1: 4*c x, y,* 1/4; Mn: 4*a* 0, 0, 0; F2 8*d x, y, z* (Rp = 0.044, Rwp = 0.063, χ^2 = 23.60 for 61 variables)

*I*4/*mcm* K: 4*b* 0, 1/2, 1/4; Mn: 4*c* 0, 0, 0; F1: 4*a* 0, 0, 1/4; F2: 8*h* *x*, 1/2-*x*, 0 (Rp = 0.054, Rwp = 0.066, χ^2 = 3.60 for 28 variables)

$Pm\bar{3}m$ K: 1*b* 1/2, 1/2, 1/2; Mn: 1*a* 0, 0, 0; F1: 3*d*, 1/2, 0, 0 (Rp = 0.061, Rwp = 0.070, χ^2 = 2.78 for 23 variables)

Figure Captions

Fig. 1 Calculated neutron diffraction data for the structural model of $KMnF_3$ in space group $B2_1/m$ at 12 K [9] and observed data collected using HRPD measured at 10 K. **Fig. 1a** The monoclinic model predicts the strong violations of the systematic absence conditions of *Pnma* at 3.403 Å (120: a-glide violation) and 3.408 Å (021: n-glide violation) which are unobserved in the collected data, and a pair of fundamental reflections at 3.725 Å, and 3.740 Å which are also absent in the measured data. **Fig. 1b** Observed and calculated data for the monoclinic model around the pseudocubic 200 reflection with the resolution function of HRPD shown as the horizontal line, and the estimated resolution of the laboratory diffractometer shown as a double-headed arrow [9]. The observed data are inconsistent with the calculated data, and hence the revision of the space group of $KMnF_3$ at 12 K from *Pnma* to $B2_1/m$ is found to be incorrect.

Fig. 2 Diffraction data collected using HRPD in the vicinity of the pseudocubic 200 reflection, red data, 105 K in the *I*4/*mcm* phase field, blue data, 65 K in the *Pnma* phase field, and magenta data in the nominal *Cmcm* phase field collected at 80 K. The predicted triplet of reflections expected for a *Cmcm* space group are not observed, and instead a weighted sum of profiles of two patterns similar to those of *I*4/*mcm* at 105 K and *Pnma* at 65 K is observed. The nominal phase III of $KMnF_3$ in space group *Cmcm* is not supported by the observed data which indicates phase coexistence between phases with space groups *I*4/*mcm* and *Pnma* in the temperature interval 75 K < T < 90 K.

Fig. 3 3a, the temperature variations of the integrated intensities of the pseudocubic 200 reflections for the *I*4/*mcm* phase (upward triangles) and the *Pbnm* phase (downward triangles) of $KMnF_3$. Open symbols indicate the single-phase regions, full symbols the phase coexistence region. The full black circles illustrate the integrated intensity sum from the two phases within the coexistence region (coex. region). 3b, the temperature dependence of the volume fraction of the tetragonal *I*4/*mcm* phase of $KMnF_3$ in the coexistence region. The dashed line guide to the eye is a fit to a three-parameter sigmoid function.

Fig. 4 The temperature dependence of the integrated intensity of the purely magnetic 101 reflection (indexed on the tetragonal unit cell) normalized to the phase fraction of the orthorhombic *Pnma* phase. For temperatures below 72 K the normalized intensity follows a power law dependence with an estimated Néel temperature of 77(1) K for the *Pnma* phase, however, above this temperature, the integrated intensity increases to a maximum before dropping rapidly to zero at 90 K. Assuming the magnetic phase to be orthorhombic yields non-physical values for the Mn magnetic moment and hence we deduce the tetragonal *I*4/*mcm* phase becomes antiferromagnetically ordered in the coexistence region.

Fig. 5 Refinement quality of the (211) reflection, containing both nuclear (phase fractions of the tetragonal and orthorhombic phases are 86(1)% and 14(1)%, respectively) and magnetic intensities at T = 85 K, in the models with the magnetic moments in the tetragonal phase being perpendicular to the *c*-axis (a) and parallel to the *c*-axis (b). Insets show the (211) refection in paramagnetic region (T = 90 K) and below the magnetic transition (T = 85 K) (a)

and integrated intensity of the purely magnetic (101) reflection as a function of temperature (b).

Fig. 6 Crystal and magnetic structures of the tetragonal *I*4*/mcm* (a) and orthorhombic *Pn'ma'* (b) phases of $KMnF_3$. The primary *G*-type antiferromagnetic mode is shown by red arrows while the symmetry allowed, in the case of *Pn'ma'* magnetic space group, secondary A_x- and F_y-modes by blue and black arrows, respectively.

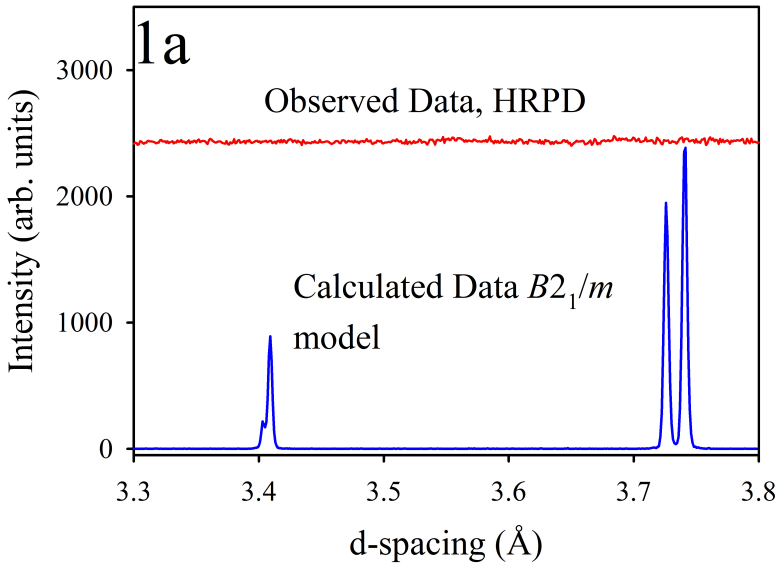
1a
Observed Data, HRPD
Calculated Data $B2_1/m$ model
Intensity (arb. units)
d-spacing (Å)
0
1000
2000
3000
3.3
3.4
3.5
3.6
3.7
3.8

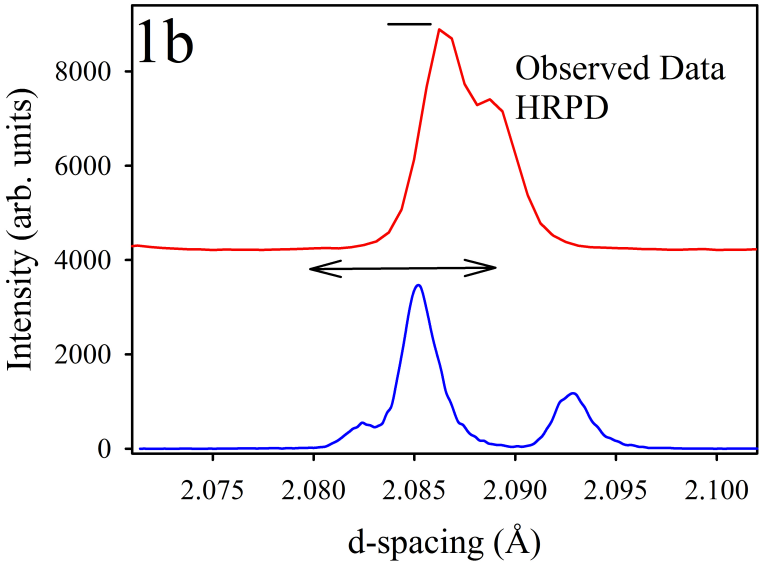
1b
Observed Data
HRPD
Intensity (arb. units)
d-spacing (Å)
0
2000
4000
6000
8000
2.075
2.080
2.085
2.090
2.095
2.100

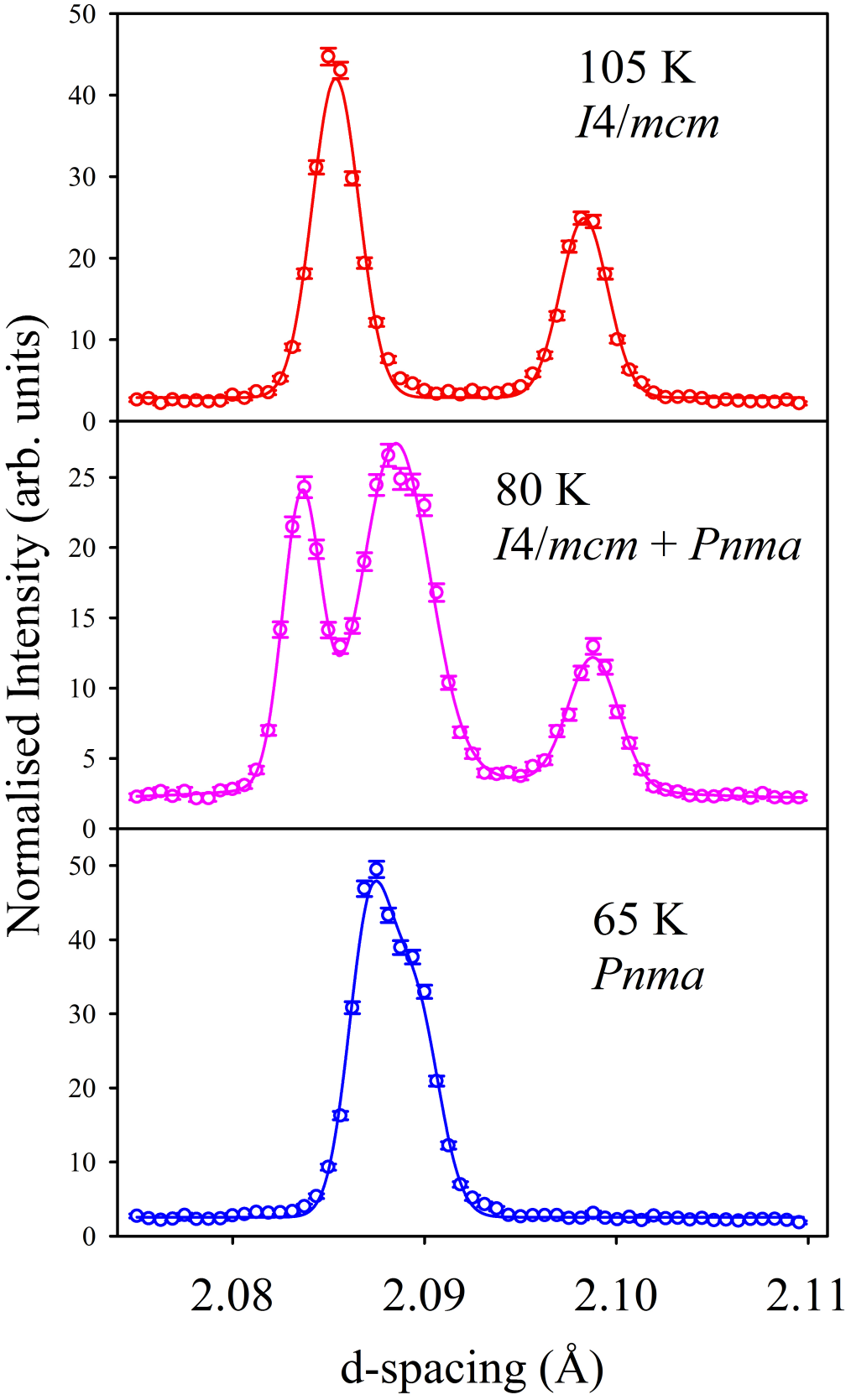
105 K
I4/mcm
80 K
I4/mcm + Pnma
65 K
Pnma
Normalised Intensity (arb. units)
d-spacing (Å)
2.08
2.09
2.10
2.11

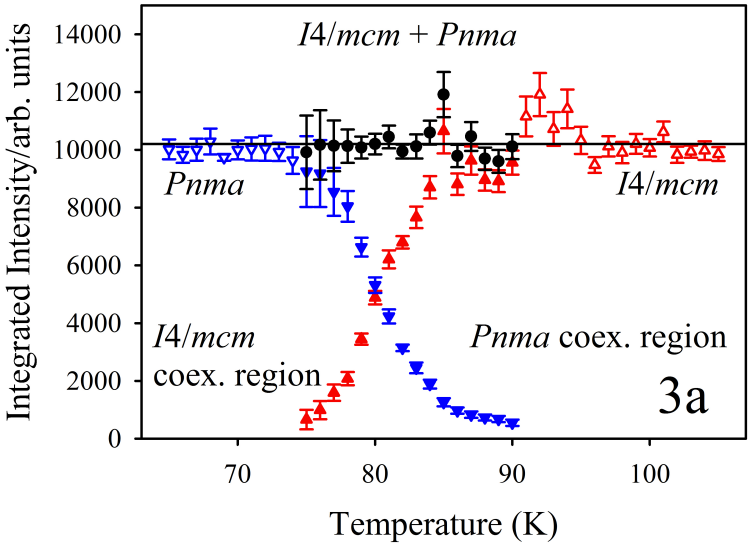
I4/mcm + Pnma
Pnma
I4/mcm
I4/mcm
coex. region
Pnma coex. region
3a
Integrated Intensity/arb. units
Temperature (K)

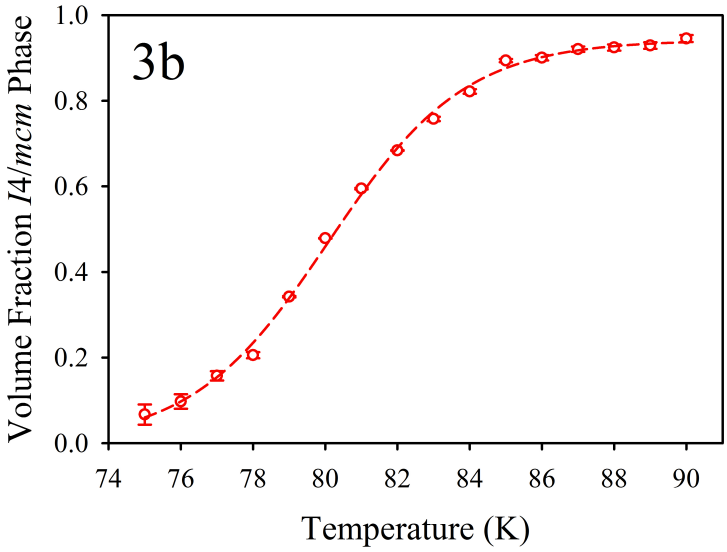
3b
Volume Fraction I4/mcm Phase
Temperature (K)

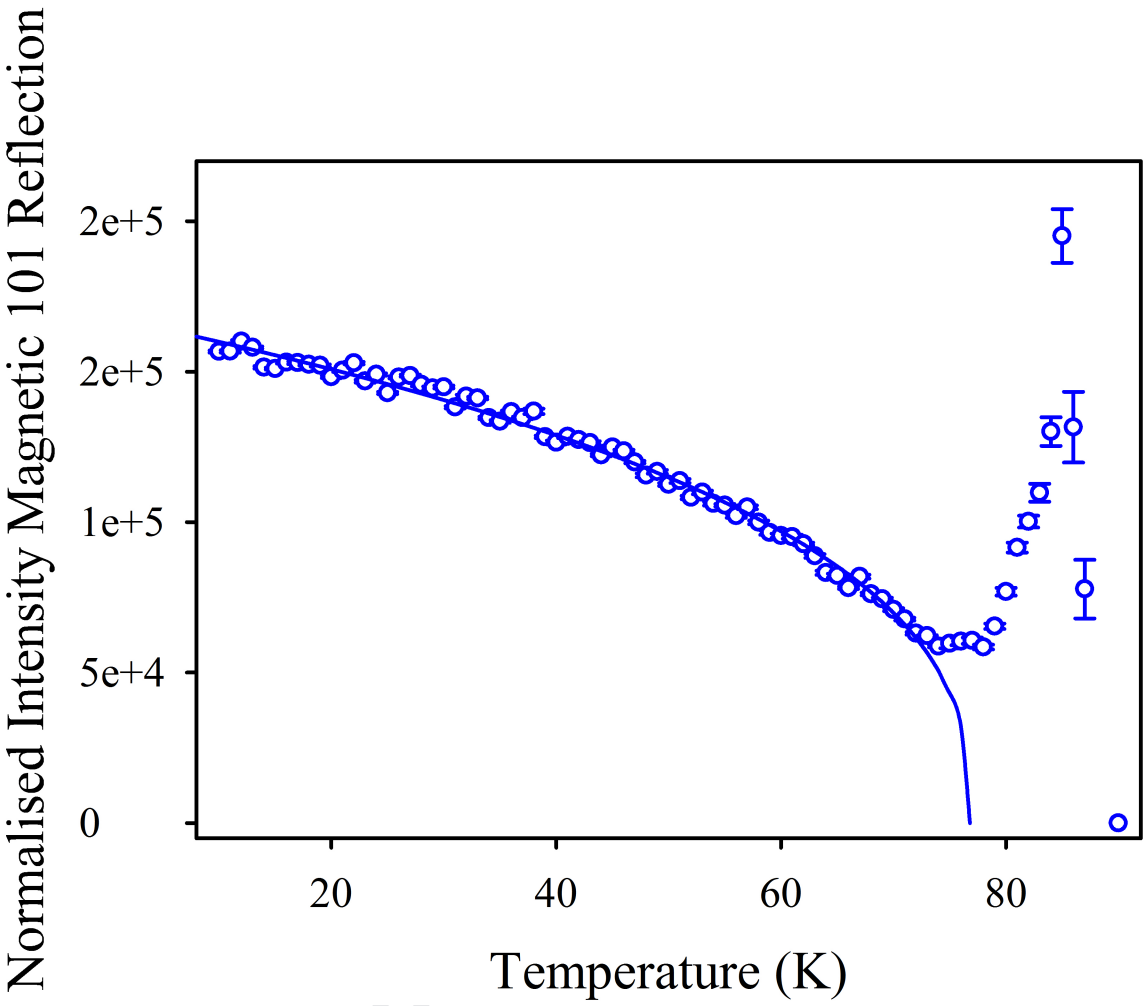
Normalised Intensity Magnetic 101 Reflection
2e+5
2e+5
1e+5
5e+4
0
20
40
60
80
Temperature (K)

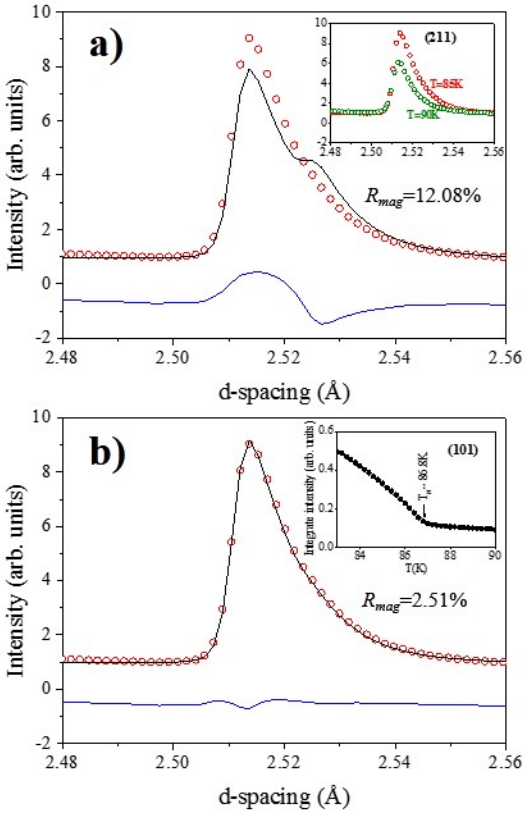

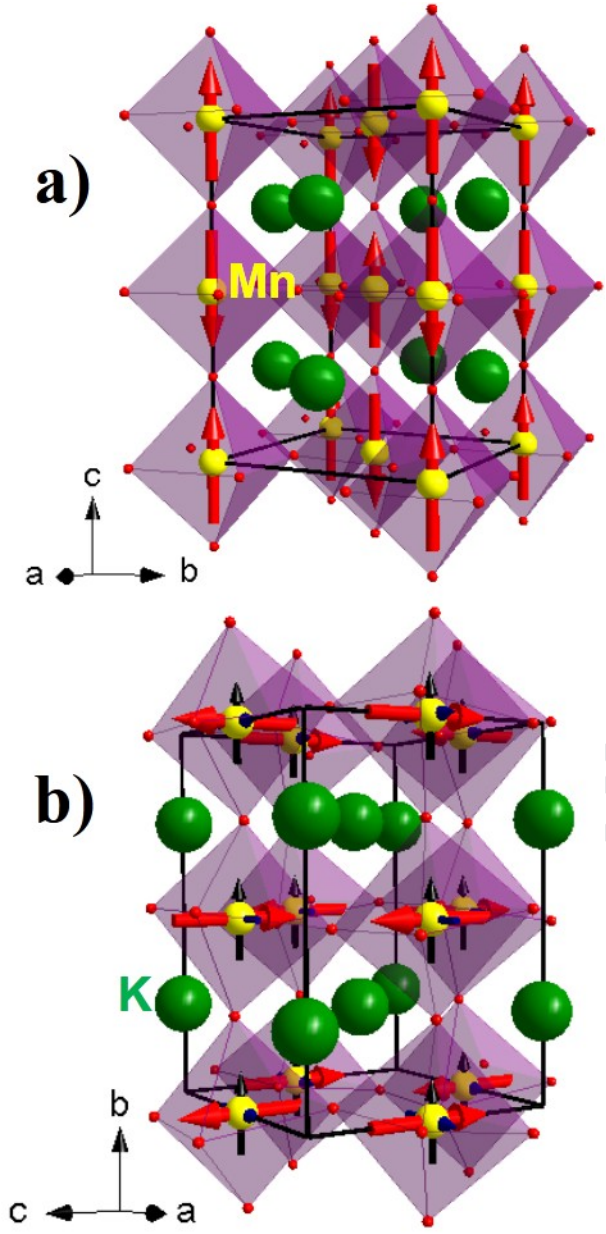

- Phase III of $KMnF_3$ shown to be phase coexistence of phases I and IV
- Collinear antiferromagnetic structure reported in Shubnikov group *I*4/*mcm*
- Canted antiferromagnetisc structure reported in Shubnikov group *Pn′ma′*
- Recent revision of space group of phase IV from *Pnma* to $B2_1/m$ is shown to be incorrect

On behalf of my co-authors, I declare that

- The article is original.
- The article has been written by the stated authors who are all aware of its content and approve its submission.
- The article has not been published previously.
- No conflict of interest exists.
- If accepted, the article will not be published elsewhere in the same form, in any language, without the written consent of the publisher.